Optical Flow for Motion Images with Large Displacement by Functional Expansion

Jin-Woo Kim[†]

ABSTRACT

One of the representative methods of optical flow is a gradient method which estimates the movement of an object based on the differential of image brightness. However, the method is ineffective for large displacement of the object and many improved methods have been proposed to copy with such limitations. One of these improved techniques is the multigrid processing, which is used in many optical flow algorithms. As an alternative novel technique we have been proposing an orthogonal functional expansion method, where whole displacements are expanded from low frequency terms. This method is expected to be applicable to flow estimation with large displacement and deformation including expansion and contraction, which are difficult to cope with by conventional optical flow methods. In the orthogonal functional expansion method, the apparent displacement field is calculated iteratively by a projection method which utilizes derivatives of the invariant constraint equations of brightness constancy. One feature of this method is that differentiation of the input image is not necessary, thereby reducing sensitivity to noise. In this paper, we apply our method to several real images in which the objects undergo large displacement and/or deformation including expansion. We demonstrate the effectiveness of the orthogonal functional expansion method by comparing with conventional methods including our optimally scaled multigrid optical flow algorithm.

Keywords: Optical flow, orthogonal functional expansion, multigrid, deformation

1. INTRODUCTION

Methods for estimation of velocity field (optical flow) from motion images have been proposed by many researchers. They are classified mainly into two categories ; gradient method[1-5] and correlation method[6]. The gradient method assumes that brightness of a tracked point on a target object is not changed during motion. Under this assumption, the method uses the differential continuity equation to calculate small displacement in direction of the brightness gradient. Then, component of the displacement field perpendicular to the brightness gradient is determined by regularization utilizing

※ Corresponding Author : Jin-woo Kim, Address : (608-736) 314-79 Daeyeon-Dong, Nam-Gu, Busan, Korea, TEL : +82-51-607-5153, FAX : +82-51-625-1402
E-mail : jinwoo@ks.ac.kr
Receipt date : July 5, 2004, Approval date : Oct. 28, 2004
[†] Dept. of Multimedia Eng., Kyungsung Univ.

a smoothness constraint[7,8]. However, the gradient method has a problem that the displacement should be smaller than a scale length of the brightness gradient. Therefore, the estimation error becomes large for large displacements. The multigrid (multi-resolution) method[9-16] is a powerful counter measure to cope with this problem. For example, S.Ghosal et al[17] proposed a method of combining the gradient method with an isotropic smoothness constraints and the multigrid method. However, the multigrid method has a problem with how well the velocity of the higher resolution level is estimated from the lower resolution level. In the standard multigrid method, the finer resolution level velocity is estimated from the coarser level using a fixed scale factor. The optimally scaled multigrid method proposed by us generates the higher resolution level image using the estimated flow with various scales and determine the in-

terlevel scale under the criterion of least squared error between the real second image and the estimated second image. By this we can calculate a flow for a large displacement. However, there is a tendency that the accuracy is decreased for large displacement or motion with rotation. On the other hand, though the correlation method can measure even the large displacement, it requires the identification of the pattern. Further, when there is a deformation of such as rotation or enlargement, its application becomes difficult or its coping with becomes complicated. Moreover, to avoid the differentiation of noisy images, SSD (sum-of-squared difference) method has been proposed[18]. This is a region-based matching method, and this has a characteristic of correlation method to some extent as well as the differential techniques[19]. Another constraints of epipolar[20], qualitative[21], and stochastic[22,23] etc, are also employed for obtaining correspondences or tracking in image sequence.

Against this, we proposed an orthogonal functional expansion method (OFEM) which is quite different from the conventional approaches. The constraint used is the integral transform value of image brightness being constant. The OFEM is a top down approach expanding the motion of the whole image in turn from a low frequency. Thus the OFEM has a feature in the point that the motion itself is divided naturally into multiscales using the weight functions. It uses a linealized integral transform equation as a constraint, and the motion is obtained by using projection method onto the convex set (pocs). Though the method is expected so that it is also applicable to the case where the object is largely deformed including large displacement, deformation, and rotation, with keeping its brightness.

In this paper, applying our OFEM to real images with large translation, enlargement, and rotation, comparing with Horn & Schunck method, multigrid method, and optimally scaled multigrid method, we show that the orthogonal functional expansion method can obtain good flow even for natural images where the constraint of the integral value of the brightness being constant is not necessarily guaranteed.

The organization of this paper is as follows : In Section.2, the outline of the OFEM is described. In Section.3, some experimental results are shown. In Section.4, some discussions and conclusions are given.

2. ORTHOGONAL FUNCTIONAL EXPANSION METHOD

If we use the brightness gradient (differentiation of image) as in the gradient method, there happens the evil effect of weekness to noise, or inability to obtain the large displacement, etc. This means that the estimation results of the optical flow are largely affected by the imaging condition. Ideally it is desirable that the system is robust as not disturbed by such external factor. The OFEM based on the constraint of invariant integral value does not need the differentiation of image, and can overcome such defects of the gradient method. In OFEM the error norm is minimized at each spatial frequency as the constraint, and the motion is calculated by the projection method onto the convex set (pocs).

2.1 Fundamental Constraint Equation

When the first image $\rho_1(\ r_1\ )$ is changed to the second image $\rho_2(\ r_2\ )$, the motion can be regarded as the coordinate transformation $r_2 = r_1 + s(\ r_1\ )$, and the image brightness is related by the following equation :

$$\rho_2(\ r_2\ ) = \rho_1(\ r_1\ ) \tag{1}$$

In this case, we have the following two equations which should become equal :

$$I_n \equiv \int_{img2} g_n(\ r_2\ )\rho_2(\ r_2\ )d\ r_2$$

$$= H_n(s) = \int_{img1} J_D(r_1) g_n(r_1 + s) \rho_1(r_1) d r_1$$
$$; n = 1, 2, \cdots, N \tag{2}$$

where *img1* is a domain to be processed, and *img2* is a range corresponding to it. The area correction factor $J_D(r_1)$ is a determinant of the Jacobian matrix $J_{ij}(r_1)$:

$$J_{ij} = \frac{\partial r_{2j}}{\partial r_{1i}} = \delta_{ij} + \frac{\partial s_j(r_1)}{\partial r_{1i}}$$
$$; i, j = 1, 2, \cdots$$

Eq.(2) is the fundamental integral constraint equation of OFEM, and each term expresses the functional expansion coefficient of the brightness distribution $(\rho_1(r_1)$ or $\rho_2(r_2))$ by an arbitrary function $g_n(r_2)$. That is, it expresses a necessary condition that the expansion coefficient by $g_n(r_2)$ of the image $\rho_2(r_2)$ after the displacement should be equal to the expansion coefficient with $g_n(r_1 + s)$ spacially deformed by the displacement s of the image $\rho_1(r_1)$ before the displacement. In this method, we do not make coincide directly the displaced first image with the second image, but coincide the coefficients by $g_n(r)$: $n = 1, 2 \cdots$ By this, instead of differentiating the noisy image, we can do with differentiating $g_n(r)$ beforehand by selecting differentiable cardinal functions $\{g_n(r)\}$ such as a set of orthogonal functions. This becomes the biggest merit comparing with the gradient method. Further, the OFEM can include naturally the multigrid method which is effective to the large displacement of the object.

2.2 Displacement Estimation by Norm Minimization

From Eq.(2), we have $I_n = H_n$. Assume now the displacement field $s(r_1)$ is shifted by unknown quantity $\delta s(r_1)$ from the known quantity $s_0(r_1)$, and the corresponding each quantity is also divided into the known quantity and the unknown quantity as follows :

$$s = s_0 + \delta s$$
$$H_n(s) = H_n(s_0) + \delta H_n$$
$$J_D(r_1) = J_0(r_1) + \delta J(r_1)$$

By dividing the each quantity into the known term and the unknown term, and expanding $H_n(s)$ in Eq.(2) by the first-order Taylor series, we have the following linearized integral constraint equation :

$$\triangle H_n = H_n(s) - H_n(s_0)$$
$$= \int_{img1} \left[J_0(r_1) \left[\frac{\partial g_n(r_1 + s_0)}{\partial s} \right] \delta s + g_n(r_1 + s_0) \delta J \right] \rho_1(r_1) d r_1 \tag{3}$$

Here we define norms in the scalar field $a(r)$ and the two-dimensional field $(a(r), b(r))$ by the following equations :

$$\|a(r)\|^2 = \int \rho(r) |a(r)|^2 d r \tag{4}$$

$$\|(a(r), b(r))\|^2 = \|a(r)\|^2 + \|b(r)\|^2 \tag{5}$$

Now, we define a cost function as follows :

$$C = \|\delta s\|^2 + \alpha^2 \|\delta J\|^2$$
$$= \int_{img1} \rho_1(r_1) (|\delta s_x|^2 + |\delta s_y|^2 + \alpha^2 |\delta J|^2) d r_1 \tag{6}$$

where, $\delta s = (\delta s_x, \delta s_y)$ and α^2 is a non-negative weighting factor. By minimizing this cost function, the unknown displacement δs and δJ are following Eq.(7) and (8) :

$$\delta s_n(r_1) =$$
$$\frac{\alpha^2 [I_n - H_n(s_0)]}{\alpha^2 \| J_0(r_1) g_{ns} \|^2 + \|g_n\|^2} J_0 g_{ns}(r_1 + s_0) \tag{7}$$

$$\delta J_n(r_1) =$$
$$\frac{[I_n - H_n(s_0)]}{\alpha^2 \| J_0(r_1) g_{ns} \|^2 + \|g_n\|^2} g_n(r_1 + s_0) \tag{8}$$

where, $g_{ns} = (g_{nx}, g_{ny})$, derivative of g_n by s. The estimated displacement and area correction

factor can be computed by iterative projections onto the solution space of each linealized integral constraint equation. This technique is commonly referred to as convex projections or projections onto convex sets (pocs). We can see that the unknown displacement $\delta s(r_1)$ obtained by g_n turns to the direction of the gradient of the weighting function g_n. The displacement $s_0(r_1)$ and area correction factor $J_0(r_1)$ are updated at each projection as follows :

$$s_0(r_1) \Leftarrow s_0(r_1) + \delta s(r_1) \qquad (9)$$

$$J_0(r_1) \Leftarrow J_0(r_1) + \delta J_n(r_1) \qquad (10)$$

3. EXPERIMENTAL RESULTS

Seven kinds of experiments have been performed including displacement with enlargement, shift, and rotation. The following orthogonal functions were tested as the integral constraint :

(1) Trigonometric function $\sin(kx)$ and $\cos(qx)$:

There arises the discontinuity at both end of the cos term, and it caused a large error in the expansion.

(2) Triangle-shaped Walsh function :

In order to make differentiable, though we modified the Walsh function to triangle shape, the error was large.

(3) Adjoint Hermit function[24] :

It becomes a sum of the normal distribution function. Though at the central part of each function, the accuracy of the differentiation is high, at the both ends of the function it takes small values and the merit of the functional expansion becomes decreased.

(4) Trigonometric function $\cos(kx)\cos(qy)$ and $\sin(kx)\sin(qy)$:

The drawbacks of (1)-(3) were removed.

Thus, since the results of (4) were the best, we only describe about (4) in the followings using FFT : The evaluation of the OFEM was performed by comparing it with *Horn* and *Shunck* method,

multigrid method, and optimally scaled multigrid method. The comparison of the four methods are carried out mainly by evaluating the similarities between the original second image and an estimated second image which is generated using the original first image and the optical flow obtained by each method. Lin et al.[25] evaluated nine kinds of image interpolation methods by *RMS errors* of the several image pairs and several optical flow estimation methods. In this paper, though we estimated the second image using only bilinear interpolation, we think from the comparisons of the results of the calculated flows that the general tendency of the results using another interpolation methods will not differ so much from our evaluation results.

The obtained optical flows are shown with average of nine pixels at intervals of three pixels, and with the velocity scale of 1.0. Two evaluation criterions of normalized *RMS (NRMS) error* and *correlation value (COR)* are adopted. These evaluation values are shown in (11) and (12).

$$NRMS\ error = \sqrt{\frac{\sum x \sum y (\rho_2(x,y) - \hat{\rho}_2(x,y))^2}{\sum \sum \rho_2{}^2(x,y)}} \times 100(\%) \qquad (11)$$

$$COR = \frac{\sum x \sum y [\rho_2(x,y) - \bar{\rho}][\hat{\rho}_2(x,y) - \bar{\hat{\rho}}_2]}{\sqrt{\sum x \sum y [\rho_2(x,y) - \bar{\rho}]^2}\sqrt{\sum x \sum y [\hat{\rho}_2(x,y) - \bar{\hat{\rho}}_2]^2}} \qquad (12)$$

where $\bar{\rho} = [\sum x \sum y \, \rho_2(x,y)] / M \times N$, $\bar{\hat{\rho}}_2 = [\sum x \sum y \, \hat{\rho}_2(x,y)] / M \times N$. $\rho_2(x,y)$ and $\hat{\rho}_2(x,y)$ are the original second image and the estimated second image. Especially, for flow of rotating images which are the feature of this paper, *NRMS error* and *correlation value* between the original second image and the estimated second image vs. rotation angle are evaluated in this paper. Further, in the cases of shift, and shift with enlargement, with selecting a moving object manually, we tried the pattern search based on the correlation method for comparisons. Relative computation time of *Horn* and *Shunck*, multigrid, and scale optimized multigrid methods were 1 (typically 30 second by WS for

128×128 images), 1.15, 1.7, 4.3, respectively.

3.1 Shift

□ TURTLE

Original image pair of the first and the second images of Turtle used in the experiment are shown in Fig. 1, where the object is displaced right hand side by 18 pixels. The size of the whole image is 128×128 and object size is 71×38.

Optical flow obtained by applying the four methods to Fig. 1 is shown in Fig. 2 (a)-(d). We can see that in the case of *Horn & Schunck* method, the optical flow is not detected at all. In the case of the multigrid method, flow error is large. On the other hand, in the case of optimally scaled multigrid method, the result is rather improved than the cases of *H&S* and multigrid method. In the case of OFEM, the result is much improved.

□ KOALA

In Koala (Fig. 3) the object is moved left up direction along x-axis and y-axis by 31 and 33 pixels, respectively. The object size is 26×38. Fig. 4 (a)-(d) are optical flows obtained by applying the four methods to the first and the second images. We can see that the flow is hardly estimated in Fig. 4 (a)-(c). In OFEM, optical flow could be calculated to some extent as a whole.

In Table 1, *RMS errors* and *correlation values* are shown. Also in this experiment, there are large errors of flows in the *Horn & Schunck* method, the multigrid method, and the optimally scaled multigrid method. This is because the displacement is too large to be calculated correctly by applying the *Horn & Schunck* method, the multigrid method, or the optimally scaled multigrid method. However, in the OFEM case, the whole tendency of the flow could be estimated well than the other methods, and concerning the *RMS error* and *correlation value* the OFEM is also superior to the other methods.
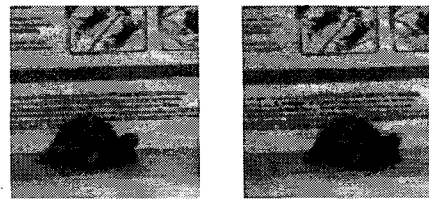
(a) First image   (b) Second image

Fig. 1. Selected frames of the experimented Turtle image sequence.

(a)   (b)
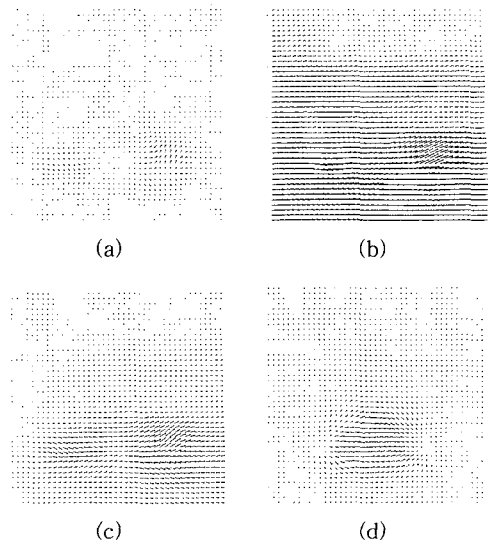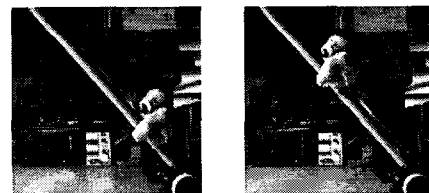
(c)   (d)

Fig. 2. Estimated flow of Turtle sequence using four optical flow methods. (a)Horn & Schunck's method, (b)standard multigrid method, (c)scaled multigrid method, (d) OFEM.

(a) First image   (b) Second image

Fig. 3. Selected frames of the experimented Koala image sequence.

3.2 Rotation : Rubic Cube and Hamburg Taxi

The optical flow with rotation is not easy to obtain since it includes complex factors. Rubic cube images (No. 4 and No. 19) are shown in Fig. 5, whose
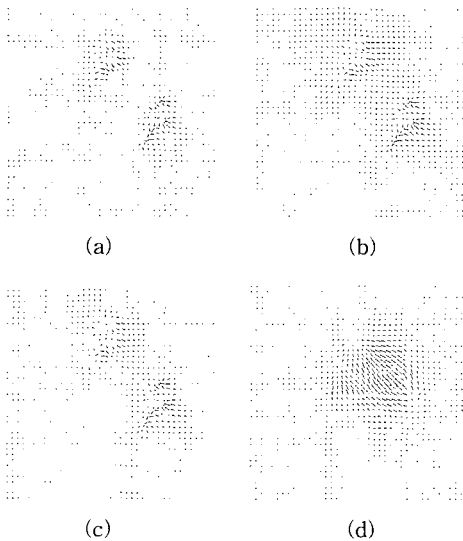
(a)

(b)

(c)

(d)

Fig. 4. Estimated flow of Koala sequence using four optical flow methods. (a)Horn & Schunck's method, (b)standard multigrid method, (c)scaled multigrid method, (d) OFEM.

Table 1. Comparison of NRMS error's and correlations between original and estimated second image using estimated flows.

| Comparison of the methods		Sample images			
		Turtle	Koala	Jan	Robot
Horn & Schunck	NRMSE	33.778	34.871	22.022	35.524
	Correlation	0.660	0.818	0.705	0.853
Standard multi-grid	NRMSE	23.874	34.641	21.977	35.411
	Correlation	0.793	0.821	0.709	0.854
Scaled multi-grid	NRMSE	22.538	34.423	20.932	35.355
	Correlation	0.806	0.824	0.739	0.855
OFEM	NRMSE	14.594	20.904	18.574	22.113
	Correlation	0.909	0.937	0.868	0.944
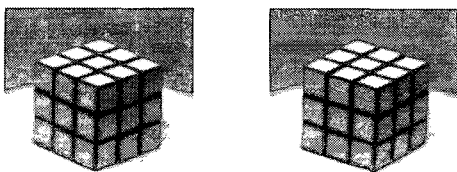
(a) First image (No.4)   (b) Second image (No.19)

Fig. 5. Rotating Rubic cube sequence.

image sizes are both 128×128. Maximum displacement accompanying the rotation in this case is about two pixels. Making the No. 4 image the base first image, the rotation amount becomes large according to increasing the image No. of the second image. No. 10 and No. 15 of Hamburg Taxi are shown in Fig. 6 whose sizes are both 64×64. We make the No. 10 the base first image. Hamburg Taxi has motions of about four pixels left and three pixels up at the center, and about 2.5 degrees of right-handed rotation.

Fig. 7 (a)-(d) and Fig. 8 (a)-(d) are optical flows obtained by applying the four methods to the first and the second images of Fig. 5 and Fig. 6, respectively. The estimated second images generated with obtained optical flow and the first image are shown in Fig. 9 (a)-(d) and Fig. 10 (a)-(b).

In Fig. 11 and Fig. 12, the *correlation values* and the *RMS errors* are shown between the original second image and the estimated second image. In the case of the Rubic Cube, *Horn & Schunck* method except, multigrid method, and optimally scaled multigrid method could estimate the flow well, there are places where the flow could not be estimated around the corners of the Rubic Cube. This is because around the corner since not only the brightness changes rapidly, but also the displacement is the largest and relative motions with the background are largely included, and the flow estimation is difficult from the beginning. On the other hand, by the OFEM the result is fairly improved and flow is almost estimated (Fig. 7(d)). In case of the Hamburg Taxi, the flow is not detected at some places by the *Horn & Schunck* method (Fig. 8(a)). Though in cases of the multigrid method and optimally scaled multigrid method the result is fairly improved than the *Horn & Schunck* method, error is seen around the taxi(Fig. 8(b), (c)). Contrary to this, in the case of OFEM though the error is still seen a little around the taxi, we can see that the result is further improved as a whole (Fig. 8(d)). Calculated results of the *correlation values* and the *NRMS error* is shown in Fig. 11
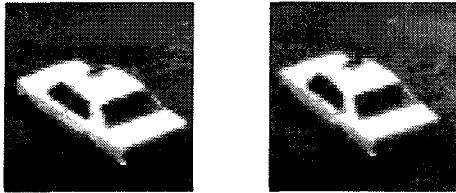
(a) First image (No.10)   (b) Second image (No.15)

Fig. 6. Rotating Hamburg Taxi sequence.

(a)   (b)
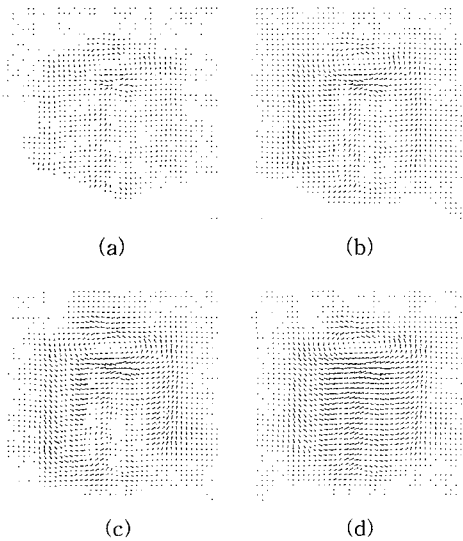
(c)   (d)

Fig. 7. Estimated flow of rotating Rubic cube se-
quence using four optical flow methods.
(a)Horn & Schunck's method, (b)standard
multigrid method, (c)scaled multigrid
method, (d)OFEM.

and Fig. 12. We can see that in cases of both
images the larger the rotation angle is, remarkably
more improved the detection accuracy of the OFEM
is than the other three methods. Also in cases of
the shift, and the enlarged shift, the larger the
displacement is, the superiority of the OFEM
becomes more dominant.

In[25], *Horn & Schunck* method (*H&S*), *Lucas
and Kanade* method (*L&K*), *Singh, and Fleet* and
Jepson method (*F&J*) are compared when bilinear
and more smooth interpolation methods are used
in the generation of the second images including
the Rubic Cube and Hamburg Taxi. Though since
besides the No's of the images are not shown in

(a)   (b)
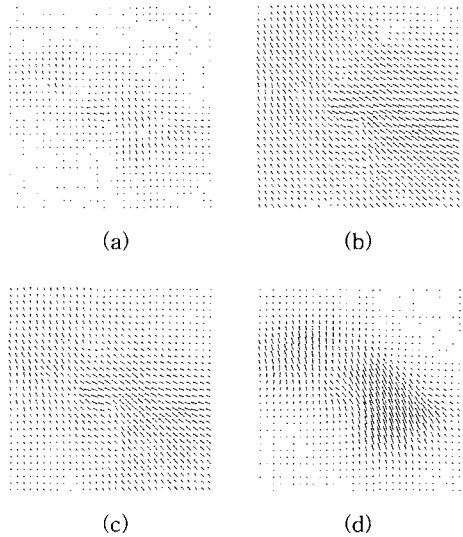
(c)   (d)

Fig. 8. Estimated flow of rotating Hamburg
Taxi sequence using four optical flow
methods. (a)Horn & Schunck's method,
(b)standard multigrid method, (c)scaled
multigrid method, (d)OFEM.

(a)   (b)
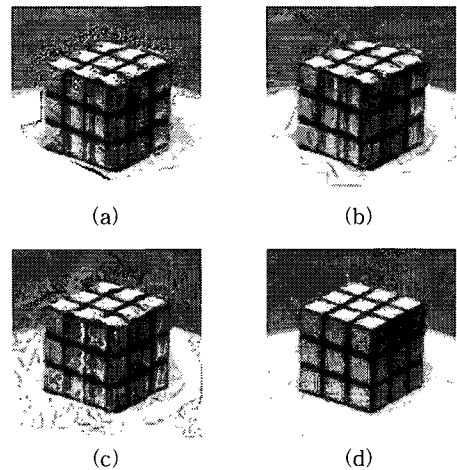
(c)   (d)

Fig. 9. Estimated images of rotating Rubic cube
sequence using four optical flow methods.
(a)Horn & Schunck's method, (b)standard
multigrid method, (c)scaled multigrid
method, (d)OFEM.

the paper, the image window sizes are different,
it is difficult to compare directly, by making the
H&S standard we compare relatively our results
and of the above four methods including with their
different parameters. In[25] the *L&K* method has

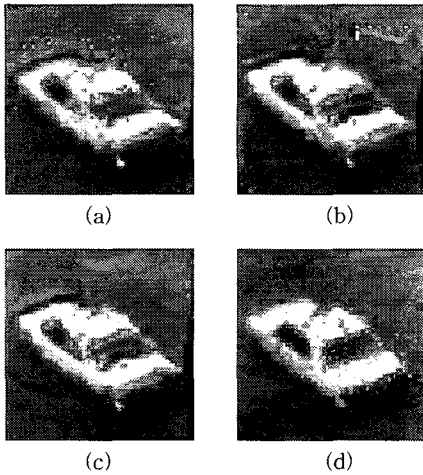(a)   (b)

(c)   (d)

Fig. 10. Estimated images of rotating Hamburg Taxi sequence using four optical flow methods. (a)Horn & Schunck's method, (b)standard multigrid method, (c)scaled multigrid method, (d)OFEM.
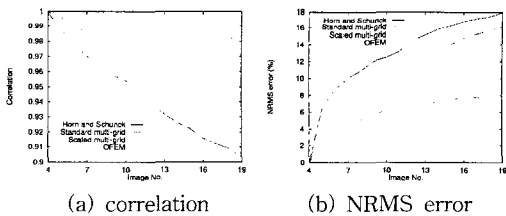

(a) correlation   (b) NRMS error

Fig. 11. Comparisons of the original and estimated second images for Rubic cube sequence using correlation and NRMS error.
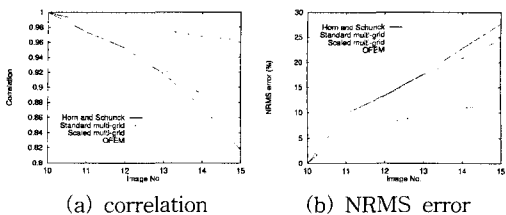

(a) correlation   (b) NRMS error

Fig. 12. Comparisons of the original and estimated second images for Hamburg Taxi sequence using correlation and NRMS error.

the least errors among the four methods, which are 41% of *H&S* in Rubic Cube. The OFEM is equal to it at the worst in any frame, and generally it's error is far less than others. Since practically we are dealing with only areas with large displace-

ment, this figure will become different when we deal with whole images including areas with small displacement. At least, however, we can say that in areas with large displacement the OFEM works effectively.

3.3 Displacement with Enlargement : Jan and Robot

Original image pairs of the first and the second images of Jan and Robot used in the experiment are shown in Fig. 13 and 14, whose sizes are both 128×128. The object sizes in the first and the second images of Jan (Fig. 13) are 20×30, 25×35, respectively, and the displaced distances are both 40 pixels, in x-direction and y-direction. The object sizes in the first and the second images of Robot (Fig. 14) are 28×25, 49×46, respectively, and the displaced distances are 56 pixels and 12 pixels, in x-direction and y-direction, respectively. Optical flows obtained by applying the four methods to Fig. 13 and 14 are shown in Fig. 15 (a)-(d) and Fig. 16 (a)-(d), respectively.

In Table 1, *NRMS errors* and *correlation values* between the original second image and the estimated
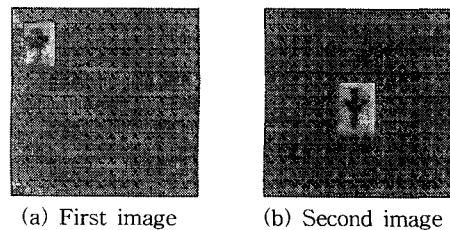

(a) First image   (b) Second image

Fig. 13. Selected frames of the experimented Jan image sequence.

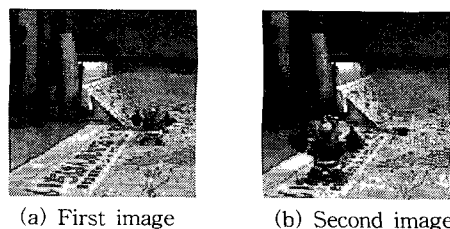(a) First image   (b) Second image

Fig. 14. Selected frames of the experimented Robot image sequence.
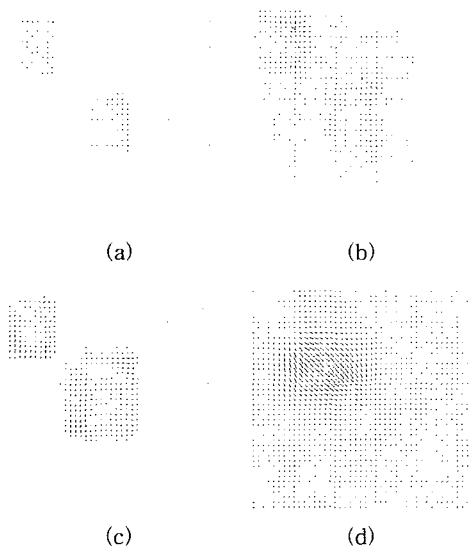
(a)   (b)

(c)   (d)

Fig. 15. Estimated flow of Jan sequence using four optical flow methods. (a)Horn & Schunck's method, (b)standard multigrid method, (c)scaled multigrid method, (d)OFEM.
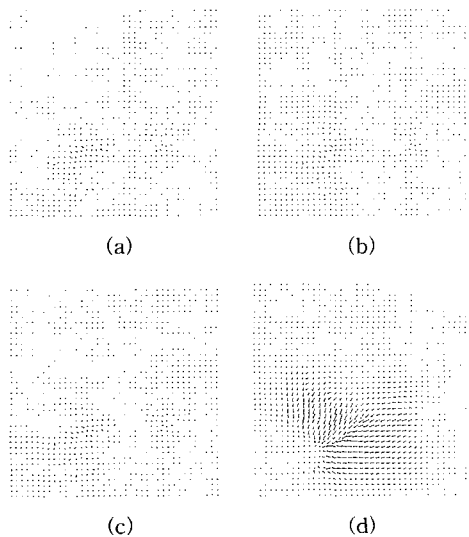

(a)   (b)

(c)   (d)

Fig. 16. Estimated flow of Robot sequence using four optical flow methods. (a) Horn & Schunck's method, (b)standard multigrid method, (c)scaled multigrid method, (d)OFEM.

second image are shown. We can see that in the cases of the gradient method, multigrid method and optimally scaled miultiresolution method, the optical flows are hardly detected. Contrary to this, in the case of OFEM, relatively good results are obtained including quantitative values. However, though the flow directions are obtained well on the whole, their sizes are not enough, and it is seen that to compensate this the tendency that pixel values are "gathered up from circumference" or "dispersed to circumference" is seen.

3.4 Comparison with Correlation Method

There are two approaches in correlation method which is a powerful technique to obtain the optical flow. One is obtaining small displacement with high precision, and the other is obtaining large motion area. In the latter, there are also two approaches of directly matching partial images and block matching under parameterized translation [26]. To cope with various types of motion, we tested only the former one. To confirm the detect ability of the correlation method, we picked out manually the moving objects as template patterns from Jan (Fig. 13), Robot (Fig. 14), Turtle (Fig. 1) and Koala (Fig. 3), Rubic Cube (Fig. 5) whose object is shifted enlarged or rotated, and made simple pattern searches by correlation method. The templates are shown in Fig. 17, respectively.

In Table 2, the maximum normalized correlation values and estimated displaced location which is the location showing the maximum normalized correlation value are shown for these cases. We can see that when the background is simple and

Table 2. Template image position search by correlation method.

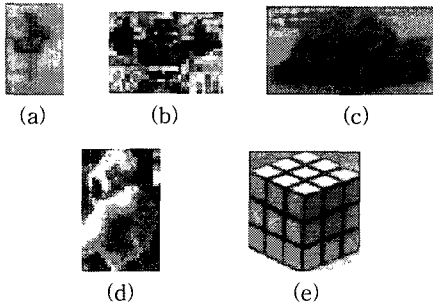| Sample images	Template image size	Position		correlation at correct position	Maximum correlation
		correct	estimated		
Jan	25×35	(51,51)	(52,51)	0.721	0.820
Robot	51×44	(18,68)	(19,72)	0.379	0.530
Turtle	71×38	(37,71)	(37,71)	0.939	0.939
Koala	26×38	(48,17)	(48,18)	0.756	0.787

Fig. 17. Selected template images. (a)Jan, (b) Robot, (c)Turtle, (d)Koala, (e)Rubic cube.

include only the shift as in the Turtle or Jan, the estimation of the displacement is easy. However, when the background is complicated and besides the object includes enlargement as in the Robot, error is caused as seen in Table 2 such that the normalized correlation value is 0.379 for the true displaced location of (18, 68) in contrast to that the maximum normalized correlation value is 0.530 for errorneously detected displaced location of (19, 72). Further if the deformation includes the 3 dimensional rotation as in the Rubic Cube or if the shape of the object is not known beforehand, it may be more difficult to detect the flow correctly. Thus, the correlation method may be effective for the simple displacement though large, or one able to be represented by such combinations. On the other hand, OFEM is effective to the large deformation where such assumption does not necessarily be applicable. We can regard these are a complementary relation.

4. CONCLUSION

By the gradient method which is the present representative optical flow method, we cannot determine the large displacement. As a method of resolving this problem we have been proposing a novel orthogonal functional expansion method (OFEM) which bases on a constraint of weighted integral of the image brightness being constant,

and determines an optical flow with the pocs method by a top-down manner. By this, instead of differentiating the noisy image, we can do with differentiating the expansion function beforehand by selecting set of differentiable orthogonal functions. This becomes the biggest merit comparing with the gradient method. Further, the OFEM can include naturally the multigrid method which is effective to the large displacement of the object.

In this paper, especially using images with large displacement, rotation, or enlargement, whose optical flow are difficult to obtain by previous methods, we have evaluated the OFEM by comparing with previous methods qualitatively and quantitatively. In order to evaluate the performance of the OFEM purely, some heuristic techniques to enhance the performance such as region/edge detection, unisotropic evaluation, or some confidence measure are not used here. Qualitatively, there still happens to cause errors around the object for the large deformations including rotation, and further such tendency is observed that enough amount of the displacement is not obtained and the shortage of the image brightness integration value is "gather up from the circumference" or "dispersed to the circumference." However, by the OFEM it is possible to obtain better optical flows as a whole. It's a common problem in optical flow algorithms that the flow size is fairly shorter than correct one for large displacement which is several times of object size. Generally speaking, the matching method is effective even for such large displacement. However, when motion is not simple, or the object rough shape is not known beforehand, it is not so easy to apply the matching method. In such cases it has been confirmed quantitatively that the OFEM can obtain better optical flow than the conventional methods for the various kinds of large displacements including rotation and enlargement. It can also be said that for small displacement, OFEM does not inferior to the conventional methods.

5. REFERENCES

[1] E. C. Hildreth, "Computations underlying the measurement of visual motion", Artificial Intelligence, 23, pp. 309-354, 1984.

[2] B. K. Horn, G. Schunck, "Determining optical flow", Artificial Intelligence, 17, pp. 185-203, 1981.

[3] H. H. Nagel, "Analysis techniques for image sequences", Proc. 4th Intern. Joint Conf. Patt. Recog, Kyoto, Japan, 1987.

[4] S. Uras, F. Girosi, A. Verri, V. Torre, "A computational approach to motion perception", Biological Cybernetics, 60, pp. 79-87, 1988.

[5] A. Mitiche, A. R.Mansouri, "On Convergence of the Horn and Schunck Optical-Flow Estimation Method", IEEE Trans on Image Processing, 13, pp. 848-852, 2004.

[6] P. Anandan, "Computing dense displacement fields with confidence measures in scenes containing occlusion", Proc. SPIE Intelligent Robots and Computer Vision Conference, 521, pp. 184, 1984.

[7] H. H. Nagel, W. Enkelmann, "An investigation of smoothness constraints for the estimation of displacement vector fields from image sequences", IEEE Trans. Patt. Anal. Mach. Intell. 8, pp. 565-593, 1986.

[8] H. H Nagel, "On the estimation of optical flo w : Relations between different approaches and some new results", Artificial Intelligence, 33, pp. 299-324, 1987.

[9] A. Brandt, "Multi-level adaptive solutions to boundary-value problems", Mathematics of Computations, 31, pp. 333-390, 1977.

[10] W. Enkelmann, "Investigation of multigrid algorithms for the estimation of optical flow fields in image sequences", Computer Vision, Graph. Image Process, 43, pp. 150-177, 1988.

[11] D. Terzopoulos, "Image analysis using multigrid relaxation methods", IEEE Trans. Patt. Anal. Mach. Intell. PAMI-8, pp. 129-139, 1986.

[12] P. J Burt, C. Yen, X. Xu, "Multi-resolution flow through motion analysis", Proceedings IEEE Computer Society on Computer Vision and Pattern Recognition, Washington/ DC, pp. 246-252, 1983.

[13] F. Glazer, "Multilevel relaxation in low-level computer vision", in Multi-Resolution Image Processing and Analysis (A. Rosenfeld, Ed.), pp. 312-330, Springer-Verlag, Berlin/Heidelberg/New York, 1984.

[14] F. Glazer, G. Reynolds, P. Anandan, "Scene matching by hierarichical correlation", Proceedings, IEEE Computer Society on Computer Vision and Pattern Recognition, Washington/ DC, pp. 432-441, 1983.

[15] R. Y Wong, E. L Hall, "Sequential hierarchical scene matching", IEEE Trans, Comput. C-27, 4, pp. 359-366, 1987.

[16] M. R. Mahzoun, Jinwoo Kim, et al, "A scaled multigrid optical flow algorithm based on the least RMS error between real and estimated second images", Pattern Recognition, 32. pp. 59-72, 1999.

[17] S. Ghosal, P. Vanek, "A fast scalable algorithm for discontinuous optical flow estimation", IEEE Trans. Patt. Anal. Mach. Intell. 18, pp. 181-194, 1996.

[18] P. Anandan, "A Computational Framework and an Algorithm for the Measurement of Visual Motion", Int. Journal of Computer Vision, 2, pp. 283-310, 1989.

[19] J. L. Barron, D. J. Fleet, S. S. Beauchemin, "Systems and Experiment Performance of Optical Flow Techniques", Int. Journal of Computer Vision, 12, pp. 43-77, 1994.

[20] J. H. Han and J. S. Park, "Contour matching using epipolar geometry", IEEE Trans. Pattern Analysis and Machine Intelligence, 22, pp. 358-370, 2000.

[21] C. J. Veenman, M. J. T. Reinders, and E. Backer, "Resolving motion correspondence for densely moving points", IEEE Trans. Pattern

Analysis and Machine Intelligence, 23, pp. 54-72, 2000.

[22] Y. Ricquebourg and P. Bouthemy, "Real-time tracking of moving persons by exploiting spatio-temporal image slices", IEEE Trans. Pattern Analysis and Machine Intelligence, 22, pp. 797-808, 2000.

[23] N. Peterfreund, "Robust tracking of position and velocity with Kalman snakes", IEEE Trans. Pattern Analysis and Machine Intelligence, 21, pp. 564-569, 2000.

[24] L. R. Lo Conte, R. Merletti, and G. V. Sandri, "Hermite expansions of compact support waveforms : Applications to myoelectric signals", IEEE Trans. on Biomedical Engineering, 41, pp. 1147-1159, 1994.

[25] T. Lin and J. L. Barron, "Image reconstruction error for optical flow", Proc. Vision Interface, May 17-20th, Banff, pp. 73-80, 1994.

[26] V. Seferdis and M. Ghanbari, "General Approach to Block-matching Motion Estimation", Optical Engineering, 32, pp. 1464-1474, 1993.
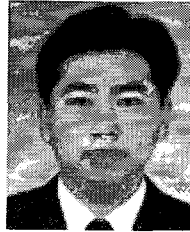
Jin-Woo Kim

He received the B.S degree in Electrical Engineering from Myongji University in 1992 and the M.S. and Ph.D. degrees in Electronic Engineering and System desigen Engineering from Fukui University, Fukui, Japan, in 1996 and 1999, respectively. From 1998 to 1999, he was a researcher at Fukui University, Fukui, Japan. From 2000 to 2003, he was a contract Professor in the Department of Information communication and Computer Engineering at Hanbat national University, Daejeon, Korea. Since 2003 he has been with the Department of Multimedia Engineering at Kyungsung University, Busan, Korea, where he is currently a full-time lecturer. His research interests include image processing, pattern recognition, and medical imaging technology.